A gas microstrip X-ray detector for application in magnetic circular dichroism experiments

J. E. Bateman,[a]* G. E. Derbyshire,[a] E. Dudzik,[b,c] G. van der Laan,[b] J. D. Lipp,[a] A. D. Smith[b] and R. Stephenson[a]

[a]CLRC Rutherford Appleton Laboratory, Chilton, Didcot, Oxon OX11 0QX, UK, [b]CLRC Daresbury Laboratory, Warrington WA4 4AD, UK, and [c]Hahn-Meitner-Institut, Glienicker Strasse 100, D-14109 Berlin, Germany. E-mail: jebpc@tn.rl.ac.uk

X-ray magnetic circular dichroism studies of magnetic 3*d* transition-metal samples require the recording of high-quality absorption scans in high magnetic fields using circularly polarized soft X-rays of energies in the range 0.5–1 keV. Normally this is performed by electron yield measurements in vacuum. This technique is rendered problematic by the influence of the high magnetic field on the motion of the electrons emitted. Detection of the fluorescent X-rays avoids this problem and eases the constraints of sample preparation and environment. However, the specifications required for a successful X-ray detector are severe, requiring an insensitivity to magnetic fields up to 4 T (for hysteresis curve measurements), a large dynamic range, detection of soft X-rays with good efficiency and signal to noise and containment of the detector structure within a space of a few cm^3. Such a detector has been developed using gas microstrip technology and tests show that these requirements can be met.

Keywords: gas microstrips; X-ray detectors; X-ray magnetic circular dichroism.

1. Introduction

X-ray magnetic circular dichroism (XMCD) is a technique for the study of magnetic materials (also paramagnetic systems polarized by an intense external magnetic field). It depends on the measurement, as a function of photon energy, of the difference in the absorption coefficient for X-rays of opposite circular polarization, which in many cases of interest can be relatively large and easily observable in the vicinity of an absorption edge (van der Laan & Thole, 1991). XMCD has rapidly gained considerable popularity because of its attractive features, which include element specificity (through choice of the absorption edge) and high sensitivity (the technique allows the detection of the magnetization even in subatomic layers of magnetic material). A further attractive feature of this novel technique is the possibility of extracting precise quantitative information on the local magnetic moments, thanks to theoretical results known as *sum rules* (Thole *et al.*, 1992).

XMCD studies of magnetic 3*d* transition-metal samples require the recording of high-quality absorption scans in high magnetic fields using circularly polarized soft X-rays of energies in the range 0.5–1 keV. Normally this is performed by electron yield measurements in vacuum. This technique is rendered problematic by the influence of the high magnetic field on the motion of the electrons emitted. Detection of the fluorescent X-rays avoids this problem and eases the constraints of sample preparation and environment. However, the specifications required for a successful X-ray detector are severe, requiring insensitivity to magnetic fields up to 4 T (for hysteresis curve measurements), a large dynamic range, detection of soft X-rays with good efficiency and signal to noise and containment of the detector structure within a space of a few cm^3. These demanding specifications can be met by a carefully designed gas microstrip detector (GMSD) such as is described below.

The GMSD introduced by Oed (1988) is a gas avalanche detector in which the fine metal high-voltage electrodes responsible for the gas gain are laid down by lithographic techniques on a glass substrate. The interleaved anode and cathode strips provide a uniform gas gain at one face of a planar X-ray detecting volume defined by a drift electrode placed parallel to the electrode plate. Many years of development of this device for demanding applications in particle physics (see for example Bateman *et al.*, 1994) have made available a mature technology now applied to X-ray detection in experimental beams at synchrotron radiation sources (Bateman, Connolly, Derbyshire, Duxbury, Lipp, Mir, Stephenson, Simmons *et al.*, 1999). Of particular importance to the present application is the planar nature of the electric drift field which transports the X-ray-generated ion clouds to the electrode array and the insensitivity of the gas gain to the shape of the drift electrode (Bateman, Connolly, Derbyshire, Duxbury, Lipp, Mir, Stephenson, Simmons & Spill, 1999). This enables the orientation of the electron drift field and the magnetic field to be accurately controlled. The monolithic self-supporting structure of the electrode plate makes it feasible to construct a successful detector within the physical limits imposed by access to the magnet vessel, namely within a tube of diameter 30 mm.

2. Operation of a GMSD in a magnetic field

Extensive experience with the operation of wire counters in high magnetic fields (up to 2 T) in applications in particle physics (Sauli, 1977) has confirmed that the presence of the magnetic field does not affect the avalanche gain but that the effect on the transport of the electrons can be severe. In the presence of a magnetic field (**B**) the electrons experience a Hall drift which shifts the drift velocity vector by an angle α relative to the electric field (**E**) where $\tan \alpha = 2B_{\perp}w/E$. Here, $B_{\perp}$ is the component of **B** perpendicular to **E** and w is the electron drift velocity (Sauli, 1977). The new drift direction lies in the plane defined by **E** and **E** × **B**. With a typical drift velocity of 5×10^4 m s^{-1} and a magnetic field of 2 T perpendicular to a typical drift field of 2 kV cm^{-1}, this angle becomes 45°. Thus, if reliable collection of the X-ray-induced ionization is to be realised, the first requirement of a detector is to maintain **E** parallel to **B**. While this can be readily attained to first order, the solenoid field pattern will inevitably curve in the space occupied by the detector leading to transverse components. Using the flexible geometry of the GMSD plates it is possible to mount them in back-to-back pairs with **E** reversed for each member of the pair. The sectional diagram of the detector (Fig. 1) shows how this is achieved. The X-rays enter the detector parallel to the plates and are detected by plates mounted on either side of a thin insulating mount. Any transverse Hall drift which robs the active region of one plate of events pushes extra events into its partner so providing compensation. In order to achieve this configuration the drift electrode (machined out of solid stainless steel) is maintained at earth potential with the cathodes and anodes of the plates at high positive potential.

3. Detector

Fig. 1 shows a longitudinal section of the complete detector. The X-ray detecting volume is situated at the extreme right-hand side where the GMSD plates are seen edge-on. X-rays enter through a thin polymer MOXTEC window (11 mm diameter) which supports

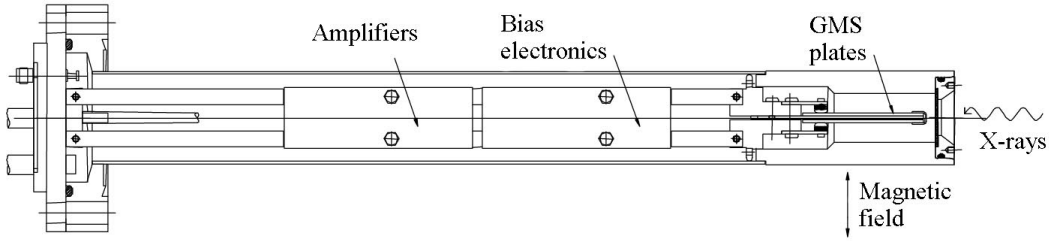

Figure 1
A sectional general arrangement diagram of the X-ray detector. The overall length of the detector is 280 mm and the diameter is 30 mm.

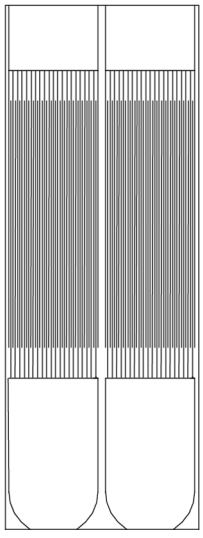

Figure 2
A reproduction of the metallization pattern on the GMSD plates used in the X-ray detector. The pattern measures 35 mm × 12 mm.

the 10^5 Pa differential pressure between the counter atmosphere and the magnet vacuum chamber. Passing through 11 mm of counter gas they arrive over the active region of the GMSD plates. Fig. 2 shows the metallization pattern of the plates used. The 10 μm-wide anode strips are connected on the plate in groups of 20 to the large pad at the bottom and the cathodes (90 μm-wide) are connected to the smaller pad at the top. The active region of the section consists of a rectangle 6 mm wide by 12 mm high. The plate on the opposite face of the central mounting is identical and the anodes and cathodes of opposite pairs are commoned to give two independent detectors, each with the symmetry property described above. The X-rays enter the detector along the direction of the electrodes.

In order to define the direction of **E**, the drift electrode must be parallel to the plates over the active area. This is achieved by machining the desired aperture from a solid stainless steel cylinder which provides the gas seal and window support at the front of the detector. The X-ray drift (conversion) gap between the plate and the stainless steel cathode is 6 mm.

Many of the essential electronic services are provided within the detector housing. Low-noise preamplifiers are mounted close to the GMSD plates thus minimizing the electronic noise and providing shaped pulses suitable for transmission to remote counting systems without loss of performance. An EHT distribution network is also provided to supply the anode–cathode potential (typically 600 V) and the drift potential (typically 1000 V) from a single input EHT supply.

Connectors on the 50 mm UHV mounting flange provide all the required electronic connections and gas ports for the flow of the counter operating gas mixture which is typically helium + 10% isobutane.

3.1. *Noise floor*

The requirement to detect X-rays of only ∼750 eV (*e.g.* cobalt *L*-shell fluorescence) imposes stringent demands on the detector. This GMSD plate was designed for another application and cannot produce high gain in the gas mixture which is imposed by the demand for efficient detection (see below). Depending on the plate design and the gas mixture, GMSDs begin to generate surface noise at a certain anode–cathode potential difference (V_{ac}) (Peskov *et al.*, 1997). This means that, as the gain increases with V_{ac}, a minimum noise floor is encountered and further increase of the gain degrades the performance. The minimum noise floor is determined by the preamplifier noise so great pains were taken to minimize the amplifier noise by careful design and fabrication. Values of the noise floor (defined as the X-ray energy threshold above which the total counting rate $\simeq$ 10 Hz) of ∼550 eV were finally obtained at a gas gain of 680 in a helium + 10% isobutane gas mixture. This was just good enough to meet the specification.

3.2. *Counting efficiency*

The determining noise source in the XMCD signal using the counter are the Poisson statistics. Thus adequate detection efficiency is a prime requisite. Two inescapable factors militate against high detection rates: (i) the very low fluorescent yield (Y) of L-shell X-rays in transition elements (∼0.003), and (ii) the small diameter of the window (11 mm) enforced by the access tube. A further attenuating factor is imposed by the dead volume of counter gas between the counter window and the active volume of the detector (11 mm path length). The dead space caused by the plates themselves also creates a loss. The efficiency of the detector was modelled by means of a Monte Carlo simulation which tracked the X-rays through the complex detector volume. Fig. 3 shows the detection efficiency as a function of the attenuation length of the counter gas (λ) for the X-ray energy in question and the distance from the XMCD sample. For 760 eV photons in helium + 10% isobutane, λ = 8.4 mm, fairly near to the optimum value. At a detector-to-sample distance of 25 mm this yields a detection efficiency of ∼0.5% of the X-rays emitted into the hemisphere towards the detector, or 0.25% when one includes the transmission of the window. Substitution of these values into a simple model for the emission of L X-rays from a thin Co sample with the circularly polarized beam on line 1.1 at the Daresbury Laboratory SRS predicts counting rates of a few kHz.

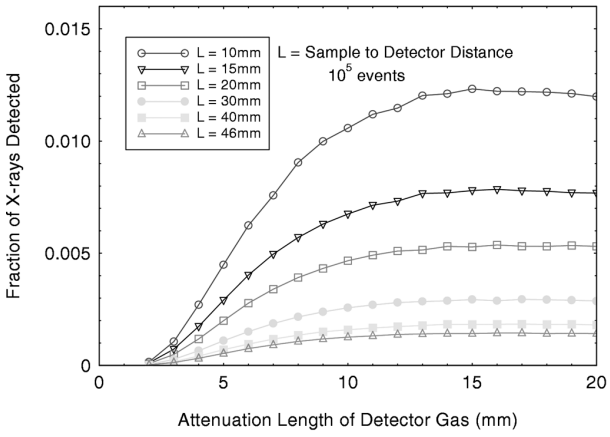

Figure 3
The results of a Monte Carlo modelling computer program which show the dependence of the X-ray detection efficiency as a function of the attenuation length of the X-rays in the counter gas and the distance of the counter from the sample.

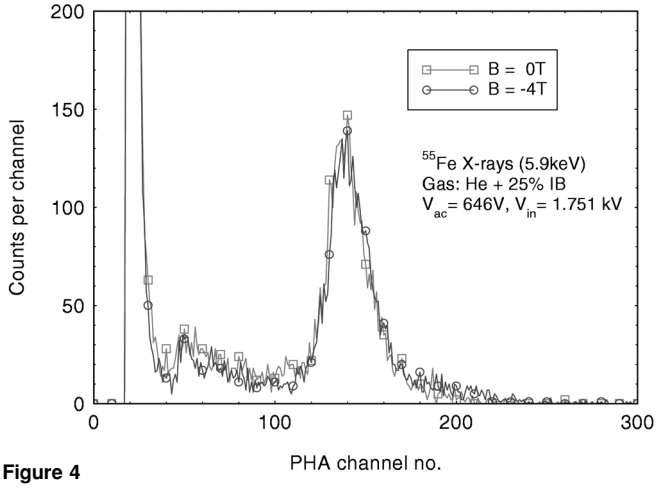

Figure 4
The pulse-height analyser spectra obtained from the X-ray counter when it is irradiated by an ^{55}Fe (5.9 keV) X-ray source. The curves are taken in position in the superconducting magnet at $B = 0$ and $B = 4$ T.

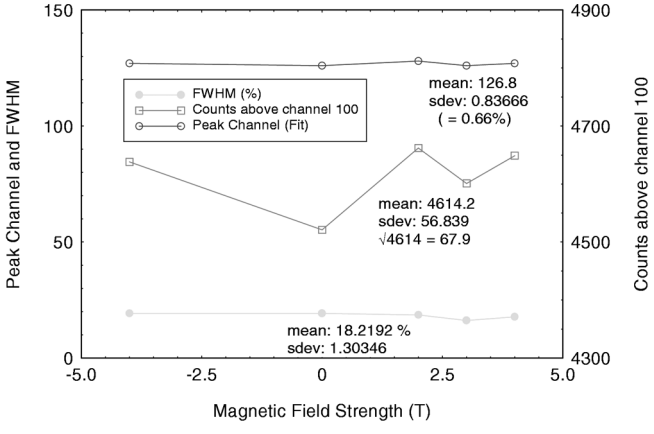

Figure 5
A summary of the performance of the energy-resolving capability of the X-ray counter in magnetic fields of -4 T $< B <$ 4 T. The peak pulse-height analyser channel, peak area and FWHM are plotted against B.

4. Detector performance in a 4 T magnetic field

The detector was installed in the superconducting magnet cryostat so that the active volume was centrally placed (*i.e.* in the maximum magnetic field) and the detector drift field aligned parallel to the magnetic field. It was irradiated by a ^{55}Fe X-ray source (5.9 keV) and operated with a gas mix of He + 25% isobutane. Pulse-height spectra were recorded over a range of magnetic field values. Fig. 4 shows the pulse-height spectra taken at $B = 0$ and $B = 4$ T. Small differences are seen but the peak channel (*i.e.* the counter gain) is seen to be invariant. Fig. 5 summarizes the results of these measurements. Over the range -4 T to +4 T the peak channel remains constant to within 0.66% (RMS) and the energy resolution remains essentially constant at 18% FWHM. In practice, the important parameter is the counting rate above a threshold. Fig. 5 shows that the counts in the peak (above channel 100) remain constant within the Poisson error.

The detector noise floor showed no dependence on the magnetic field. This is typically ∼550 eV in this gas mixture.

5. XMCD studies

For the following studies the detector was installed in the 'Flipper' magnet (Dudzik *et al.*, 2000) on beamline 1.1 at the SRS. This magnet allows the polarity of the magnetic field to be reversed quickly so that data can be taken at both polarities at the same X-ray beam energy. The magnet pole-pieces restricted the detector to a distance of 25 mm from the sample, thus reducing the sensitivity significantly. The X-ray pulses from the two detector sections were combined at the input of a discriminator which was fed into a standard data-capture system which recorded the X-ray counts, the sample leakage current (electron yield signal) and the beam monitor current. As the pulse-height analyser spectrum of Fig. 6 shows, the pulses generated by the Co L X-rays were just clear of the detector noise. A discriminator threshold setting which gave a noise counting rate of 100 Hz was estimated to detect ∼75% of the X-ray pulses.

Fig. 7 shows the results of a standard XMCD scan in which the energy of the circularly polarized X-ray beam is swept across the L_3 and L_2 edges of the Co atom. The Co sample is a 12 nm-thick layer laid down on a GaAs substrate with a 2 nm-thick Au capping layer. It is set at 45° to the X-ray beam direction. The smooth curves delineate the electron yield (sample leakage current) response and the noisier curves, the X-ray counter response with alternate magnetic polar-

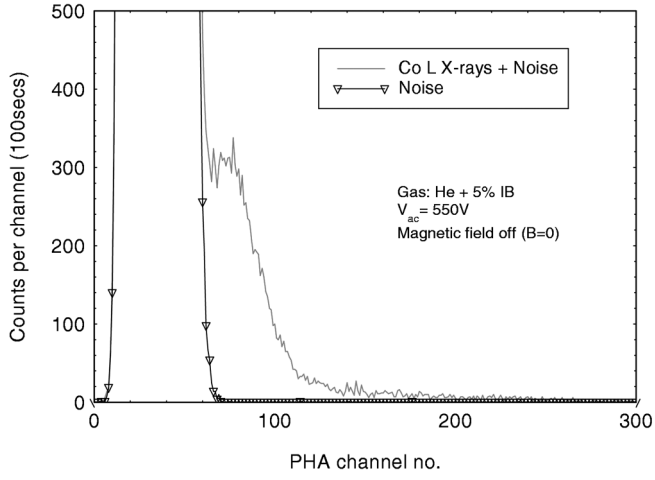

Figure 6
The pulse-height analyser spectrum obtained when the X-ray counter is irradiated by Co L X-rays (∼770 eV).

ization fields of ±0.45 T. The lower curves show the desired XMCD signal, namely the difference between the scans with alternate polarizations. Again the smooth curve is the *E*-yield signal and the noisy curve is the X-ray counting rate. The dwell time on each point is 1 s.

Fig. 8 shows the hysteresis curve obtained from the same sample with the *E*-yield (smooth) and X-ray (noisy) signals as the polarization field (B) is scanned from +0.45 T to −0.45 T while the beam energy is held constant at the L_3 absorption peak (777.5 eV). The statistics of the X-ray signal are enhanced by increasing the dwell time on each point to 5 s. Fig. 9 shows the central section of the hysteresis scan expanded by scanning over the range of $-0.0225\ \text{T} < B < +0.0225$ T. The dwell time per point is 10 s.

6. Discussion

In practical terms the X-ray detector proved very simple to set up and use. Long-term gain (and therefore sensitivity) shifts are inevitable with a flowing gas counter. While this effect can be eliminated by controlling the EHT, no problems were observed on the short time scales of the individual exposures (up to 10 min) and such elaboration is probably not required.

As Fig. 7 shows, the L_3 peak counting rate was ∼5500 Hz in line with expectations. The significant physical parameter of the measurement is the area of the difference signal. In Fig. 7 the L_3 difference ΔL_3 evaluates to 4388 counts with a Poisson error (standard deviation) of 341 counts, *i.e.* 7.8%. This indicates that more counts would be desirable. The scan in Fig. 7 took only 125 s so there would seem to be little reason not to increase the dwell time or average a large number of scans. A factor of ten in counts would reduce the error in ΔL_3 to ∼2.5%.

It will be noted that the $\Delta L_2/\Delta L_3$ ratio is noticeably less in the X-ray signal compared with the *E*-yield signal. This is a symptom of the saturation of the X-ray emission signal. The signal strength for both the X-ray and the electron signals may be approximated by the equation

$$S = \alpha N_0[1 - \exp(-\beta)], \tag{1}$$

where for X-rays $\beta_x = \mu t/\sin\varphi$ and for electrons $\beta_e = \mu R/2\sin\varphi$. μ is the linear absorption coefficient of the incoming X-rays, t is the thickness of the layer, R is the range of the auger electrons in the sample, φ is the angle of incidence (glancing), α is a constant including such things as the fluorescent yield and the detection efficiency, and N_0 is the incident beam rate. Equation (1) only displays a linear relation between S and μ for $\beta < \sim 0.1$. If one assumes that the plateau level of the signal between the L_3 and L_2 edges in Fig. 7 equates to the tabulated coefficient for Co at the L_3 edge (13.8 μm^{-1}) and that the electron signal is approximately linear, then at the peak $\mu = 144.5\ \mu\text{m}^{-1}$. Evaluating β for the present case ($t = 12$ nm, $\varphi = 45°$) gives $\beta_x = 2.46$. For electrons the L auger electron range, R, is estimated to be 2.7 nm giving $\beta_e = 0.275$. Thus the electron signal is slightly saturated and the X-ray signal is very saturated at the peak. Coming down to the plateau level between the peaks, $\beta_x = 0.32$ and $\beta_e = 0.036$. This means that the electron signal is predicted to be very slightly non-linear overall and the X-ray signal considerably so.

In the fluorescence scans the polarizing magnetic field, B, is constant and its effect on the auger electrons is not a function of the X-ray beam energy. In a hysteresis scan the field is changing continuously and the effect on the scan is quite erratic, as the sample current plot line in Fig. 8 shows. The X-ray plot is, on the other hand, a very recognisable hysteresis curve. The effect of B on the electron

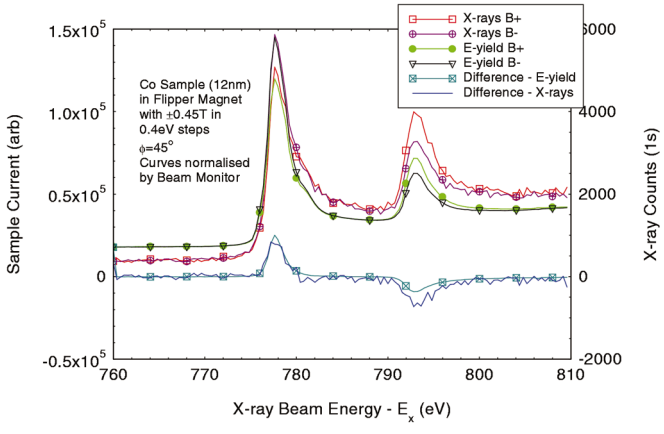

Figure 7
The XMCD fluorescence scans obtained on a 12 nm-thick sample of Co. The X-ray counts and the sample leakage current are plotted as a function of the beam energy for alternate polarizing magnetic field values (±0.45 T). The XMCD difference signals are also plotted.

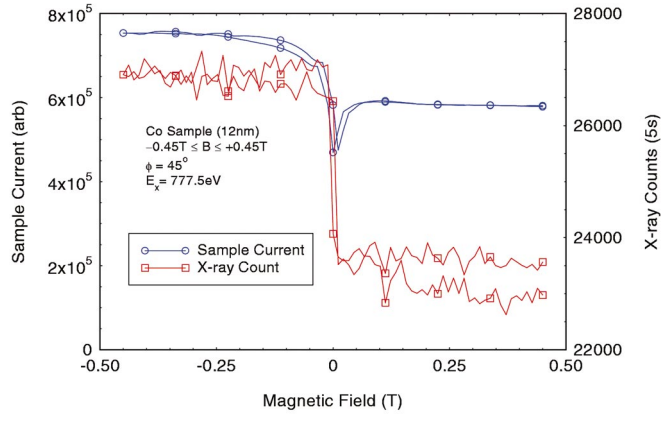

Figure 8
The XMCD signals from the 12 nm Co sample (X-ray and sample current) at the L_3 emission peak plotted as a function of the polarizing magnetic field, $-0.45\ T < B < +0.45$ T (hysteresis scan).

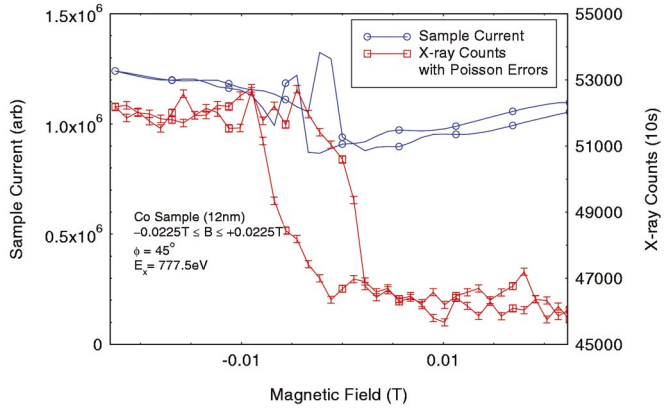

Figure 9
A fine-scale hysteresis scan of the 12 nm Co sample ($-0.0225\ \text{T} < B < +0.0225$ T).

collection is in fact resonant due to the cyclotron orbits of the electrons and, as the sampling of B is made finer (Fig. 9), more complex patterns appear in the E-yield signal. The X-ray signal remains well behaved and, with a 10 s dwell time, a satisfactory statistical error is achieved. The Poisson error bars are superimposed on the X-ray data points.

The hysteresis X-ray signal is taken on the L_3 peak so that the amplitude of the excursion, as measured, is less than it should be due to the signal saturation discussed above. The data from the fluorescence scan can be used to calibrate the saturation of the X-ray signal relative to the electron signal and the appropriate correction applied to the hysteresis data.

Data have been taken successfully on Co layers ranging from 6 nm to 50 nm. In the case of the thicker layers the saturation reveals itself as a decrease in the ΔL_3 signal which, however, remains quite measurable.

The principal improvement planned for the detector is the replacement of the GMSD plate with a new design which will reduce the gas dead space from 11 mm to 6 mm and permit a noise floor below 100 eV. The reduced noise floor will allow operation with X-rays below 500 eV if required and the reduction of the dead space will yield a factor of $\sim$2 increase in sensitivity. Further increase in the sensitivity should come from allowing the detector to approach closer to the sample. Since all other parameters are heavily constrained by physics parameters, a factor of four to five is likely to be the maximum gain from the counter design. Further improvements in statistical resolution will require longer data-acquisition times or higher beam intensities.

We thank W. Schwarzacher of Bristol University for the loan of the sample used, and I. Kirkman of Daresbury Laboratory for his assistance with the data runs.

References

Bateman, J. E., Connolly, J. F., Derbyshire, G. E., Duxbury, D. M. Lipp, J. D., Mir, J. A., Stephenson, R., Simmons, J. E. & Spill, E. J. (1999). Rutherford Appleton Laboratory Report RAL-TR-1999-057. CLRC Rutherford Appleton Laboratory, Oxon, UK (http://www-dienst.rl.ac.uk/library/1999/tr/raltr-1999057.pdf).

Bateman, J. E., Connolly, J. F., Derbyshire, G. E., Duxbury, D. M. Lipp, J. D., Mir, J. A., Stephenson, R., Simmons, J. E., Spill, E. J., Dobson, B. R., Farrow, R. C. Helsby, W. I., Mutikainen, R. & Suni, I. (1999). *Fifth International Conference on Position Sensitive Detectors*, University College, London, 13–17 September 1999.

Bateman, J. E., Connolly, J. F., Stephenson, R., Edwards, M. & Thompson, J. C. (1994). *Nucl. Instrum. Methods Phys. Res. A*, **348**, 372–377.

Dudzik, E., van der Laan, G. & Thompson, S. M. (2000). *Synchrotron Rad. News*, **13**(4), 18–22.

Laan, G. van der & Thole, B. T. (1991). *Phys. Rev. B*, **43**, 13401–13411.

Oed, A. (1988). *Nucl. Instrum. Methods Phys. Res. A*, **263**, 351–359.

Peskov, V., Ramsay, B. D. & Fonte, P. (1997). *Nucl. Instrum. Methods Nucl. Res. A*, **392**, 89–93.

Sauli, F. (1977). CERN 77-09, pp. 31–33. CERN, Geneva, Switzerland.

Thole, B. T., Carra, P., Sette, F. & van der Laan, G. (1992). *Phys. Rev. Lett.* **68**, 1943–1946.

 Received 6 March 2001 • Accepted 30 July 2001